Drying by Cavitation and Poroelastic Relaxations in Porous Media with Macroscopic Pores Connected by Nanoscale Throats (Supplemental Material)

Olivier Vincent,[1,*] David A. Sessoms,[1] Erik J. Huber,[2] Jules Guioth,[1] and Abraham D. Stroock[1,3,†]

[1]*School of Chemical and Biomolecular Engineering, Cornell University, Ithaca, New York 14853, USA*

[2]*Sibley School of Mechanical and Aerospace Engineering, Cornell University, Ithaca, New York 14853, USA*

[3]*Kavli Institute at Cornell for Nanoscale Science, Cornell University, Ithaca, New York 14853, USA*

[*] orv3@cornell.edu

[†] ads10@cornell.edu

I. SAMPLES FABRICATION

Porous silicon was prepared from p-type 1-10 Ω.cm wafers with <111> orientation. Anodization was performed using a 50:50 v:v mixture of concentrated (48%) hydrofluoric acid and ethanol, with a current density of 20 mA/cm^2. The thickness of the porous silicon layer was 5 μm, obtained with a 5 minute etch. A rapid thermal annealing step (700°C) in an oxygen-rich environment was used to improve wettability and to slow aging. Patterned features in glass were formed via standard photolithographic techniques and concentrated (48%) hydrofluoric acid etching through an annealed amorphous silicon hard mask. Silicon and glass were anodically bonded (400°C, 1200V). Filling the samples with liquid water was done in a pressure bomb with over 30 MPa of pressure to ensure the dissolution of gas nuclei. Prior to this, sample were evacuated for a few days in a vacuum chamber. Then, the samples were pre-equilibrated in a 95% relative humidity environment controlled by a saturated salt solution [1].

Two types of samples were fabricated and studied. Both consisted in a square array of 25×25 microvoids with a distance $a = 400\,\mu$m between successive voids. The geometry of the voids in glass was, respectively:

- voids 200 μm in diameter and 27 μm deep were used for strong hydraulic coupling experiments (Fig. 2, Fig 4 top in the manuscript),
- voids 50 μm in diameter and 2 μm deep exhibited weak coupling (Fig 4 bottom in the manuscript).

II. EXPERIMENTAL PROCEDURE

At the beginning of an experiment, the samples were quickly transferred to a chamber with controlled vapor activity (relative humidity). Humidity was controlled by saturated [1] or unsaturated [2] salt solutions, or with a dew point controller (Sable Systems International) with feedback from a thin film thermometer (PRT, Omega Engineering, Inc.) measuring the temperature of the backside of the sample. The drying dynamics was monitored through the transparent chamber by a stereoscope connected to a time-lapse camera (0.2 fps typically) to record the drying dynamics.

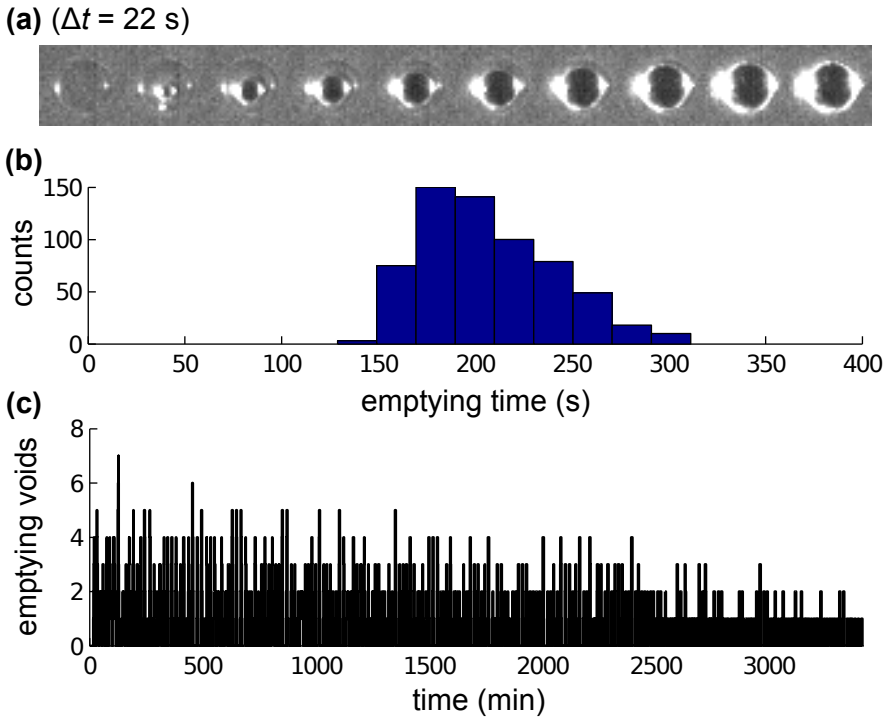

FIG. S1. (a) Emptying sequence of a single void of dimensions 200 μm in diameter and 27 μm deep. The time interval between individual images is 22 s. (b) Distribution of emptying times for the experiment presented in Fig. 2 in the manuscript. The average emptying time is $\tau \simeq 210\,\mathrm{s} = 3.5\,\mathrm{min}$. (c) Full record of cavitation dynamics extending Fig. 2b from the manuscript.

As can be seen on Fig. S1a, the nucleation and growth of individual bubbles could be monitored, allowing a measurement of the cavitation time and emptying time of each of the 625 voids from the images (Fig. S1b). The drying sequence could then be reconstructed as shown on Fig. S1c, where the number of voids in the process of emptying (i.e. containing a growing bubble) is plotted as a function of time. Fig. 2b in the manuscript is a magnification of Fig. S1c, showing the bursting phenomenon.

We considered positive feedback between cavitation events mediated by acoustic emissions. Each event did indeed emit an acoustic signal but we could rule out their potential role in triggering subsequent events because the ring-down time of these signals was short ($\sim 1\,\mathrm{ms}$) compared to the average time between cavitation events inside a burst (55 s from Fig. S1c).

III. DRYING BY CAVITATION

We exclude invasion of air from the edges of the of the sample as the mechanism for the drying observed in the reported experiments based on the following considerations:

1. Similar dynamics was observed when dehydrating the samples in a polymer (Polyethylene glycol) solution, preventing direct contact between the pore liquid and air. The development of negative pressures was then due to an osmosis phenomenon, thermodynamically equivalent to drying.

2. We measured the pore size distribution in our samples by nitrogen porosimetry at 77.3 K, showing a narrow distribution around $r_{\mathrm{p}} = 1.4$ nm of pore radius, deduced from the Barrett-Joyner-Halenda (BJH) method [3] on the adsorption curve. Using equations (1) and (2) in the manuscript with $\sigma \sim 0.072$ N/m and $\theta = 0$ leads to a typical relative humidity at which menisci will recede from the edges of $p_{\mathrm{v}}/p_{\mathrm{sat}} = a_{\mathrm{r}} = 0.47$, far below the relative humidities at which the emptying of the voids is observed ($p_{\mathrm{v}}/p_{\mathrm{sat}} = a_{\mathrm{cav}} = 0.83 - 0.86$) and below all the relative humidities used in our experiments. Even when using the upper bound of pore size ($r_{\mathrm{p,max}} = 2.3$ nm) from porosimetry and the largest contact angles reported for water on oxidized silicon $\theta_{\mathrm{max}} = 45°$ [4], the receding value $a_{\mathrm{r}} = 0.72$ is found, still far below a_{cav}.

3. The estimated liquid pressure at which cavitation occurs in our system ($P_{\mathrm{cav}} = -20$ to -24 MPa from Eq. (1)) is consistent with the cavitation pressure measured in water by various other methods such as centrifugation or acoustic cavitation [5, 6].

We note that even in the very unlikely case where bubble formation would originate from rare gas-phase invasion events and not cavitation, the drying dynamics described in this Letter would be unchanged.

IV. CAVITATION MECHANISM

The exact mechanism leading to nucleation at pressures in the range -20 to -30 MPa at room temperature is still debated [5, 6]. Indeed, using the bulk properties of water in classical nucleation theory (CNT) predicts homogeneous cavitation pressures lower than -100 MPa, close to the limit of mechanical stability, or spinodal [5, 7].

It has been shown however [8] that CNT could describe cavitation kinetics accurately by using a reduced surface tension ($\sigma \sim 0.02$ N/m) instead of the bulk surface tension ($\sigma \sim 0.07$ N/m), suggesting that cavitation is heterogeneous, and is thermally activated as assumed by CNT. This motivates the use of CNT to model nucleation kinetics in our model (see section V of the Supplemental Material).

Plausible mechanisms for heterogeneous cavitation in our system include nucleation on impurities in water, from nanoscale hydrophobic patches on the solid surfaces, or from stabilized nanobubbles. A discussion of these different mechanisms can be found in various sources [6, 9].

We note however that the results presented in this Letter do not depend on the microscopic mechanism for nucleation.

V. MODEL

Here, we describe the model of transport and cavitation kinetics that we have used to interpret and simulate our experiments.

A. Liquid Transport

In order to model the flow during drying, we begin by assuming that flow of liquid within the porous silicon satisfies Darcy's equation [10]

$$\boldsymbol{q} = -\kappa \boldsymbol{\nabla} P \tag{S1}$$

where $\boldsymbol{q}$ is the liquid volumetric flux through the porous medium, κ [m^2/(Pa.s)] is the permeability, and P [Pa] is the local hydrostatic pressure within the pore liquid.

Within this treatment, transient flows through the medium are governed by poroelasticity that can be expressed in terms of the pressure field as follows:

$$\frac{\partial P}{\partial t} = C \nabla^2 P \tag{S2}$$

where C [m^2/s] is the poroelastic diffusivity or consolidation constant. For a compressible fluid in a rigid, porous matrix, C has the form [11]:

$$C = \kappa K_{\mathrm{liq}} / \phi \tag{S3}$$

where K_{liq} [Pa] is the bulk modulus of the pore fluid. This form is appropriate for our system given that porous silicon and borosilicate glass are both much less compressible than liquid water. See section VI B for numerical values.

B. Cavitation

We model the cavitation of liquid in the macroscopic voids as a first order rate process with a rate constant, k_{cav} [s^{-1}] that depends on the hydrostatic pressure:

$$k_{\mathrm{cav}} = V_{\mathrm{void}} \times \Gamma(P) \tag{S4}$$

where V_{void} [m^3] is the volume of the void and $\Gamma(P)$ [$m^{-3}s^{-1}$] is the volumetric rate of nucleation at pressure P in the liquid.

The probability for nucleation to occur during an infinitesimal timestep $\mathrm{d}t$ is $k_{\mathrm{cav}} \times \mathrm{d}t$ while the probability for survival (no nucleation) during an observation time τ is (assuming k_{cav} constant),

$$\mathcal{S} = \exp(-k_{\mathrm{kcav}}\,\tau). \tag{S5}$$

Based on classical nucleation theory [5, 7] (CNT) we expect $\Gamma(P)$ to depend exponentially on P through the activation energy of nucleation, E_{nucl} [J]:

$$\Gamma = \Gamma_0 \exp\left(-E_{\mathrm{nucl}}(P)/k_{\mathrm{B}}T\right), \tag{S6}$$

where Γ_0 is an attempt frequency, k_{B} [$\mathrm{J\,K^{-1}}$] is the Boltzman constant, and T [K] is the absolute temperature. We chose a widely used expression for the attempt frequency [5, 7] $\Gamma_0 = k_{\mathrm{B}}T/(h \times R^*)$ where h is Planck's constant and $R^* = 2\sigma/(P - p_{\mathrm{sat}})$ the critical radius of nucleation [5, 7] (assuming that the system is evacuated from air). The activation energy is [5, 7]

$$E_{\mathrm{nucl}} = 16\pi\sigma^3/\left[3(P - p_{\mathrm{sat}})^2\right] \tag{S7}$$

In order to account for the experimental value of cavitation pressure, we use an effective surface tension σ which is lower than the bulk value for water (see section IV). We also allow this surface tension to vary from void to void in the samples to account for spatial heterogeneities. We assume that the effective surface tension belongs to a narrow gaussian distribution of mean value σ and standard deviation $\Delta\sigma$. For example, the fit of our experimental survival curve on Fig. 1e in the main text is obtained from equations S5, S6 and S7 with $\sigma = 0.0215$, $\Delta\sigma/\sigma = 0.07$ and $\tau = 1$ day.

Note that using CNT with a fixed surface tension would predict a survival curve that is an order of magnitude steeper around the cavitation transition. As a result of this decreased ΔP_{cav}, the predicted drying fronts would be sharper than observed experimentally (see section V C), but the general conclusions presented in this paper would be unchanged.

C. Dimensionless driving force and width of the cavitation front

Due to the stochastic nature of nucleation, drying by cavitation does not occur at a fixed pressure but in a range of pressure ΔP_{cav} around P_{cav}. We assume that the width Δx of the cavitation front is set by these fluctuations, so that $\Delta x \sim \Delta P_{\mathrm{cav}}/\left(\partial P/\partial x\right)$. Since the boundary pressure is fixed at P_{b} and the pressure at the cavitation front is close to P_{cav},

the pressure gradients scale as $\partial P/\partial x \sim (P_{\mathrm{cav}} - P_{\mathrm{b}})/d$ where d is the distance between the drying edge and the cavitation front (we assume a 1D geometry for the sake of simplicity). Using the definition of the dimensionless driving force $\delta = (P_{\mathrm{cav}} - P_{\mathrm{b}})/\Delta P_{\mathrm{cav}}$ comes the simple result $\Delta x \sim d/\delta$. This shows that δ is a natural measure of the driving force in the system.

VI. SIMULATIONS

A. Procedure

We simulated the drying of the extreme ink-bottles samples using an explicit finite difference (FD) scheme to solve Eq. S2 for P with stochastic cavitation events based on the pressure-dependent probability at each time step

$$\Sigma(P) = k_{\mathrm{cav}}(P) \times \Delta t \tag{S8}$$

where Δt is the time step used in the simulation and k_{cav} is from Eq. (S4). The initial condition was a uniform pressure that corresponds to the relative humidity (RH) with which the system was initially equilibrated (Eq. 1 in the main text). The boundary nodes were then held at the pressure P_{b} that corresponded to the RH to which the sample was exposed during drying. We neglected mass transfer resistance outside the porous matrix (i.e., between the air and the edge of the sample). We defined an array of void-nodes within on a square grid of FD nodes. While filled with liquid, a single pressure was assigned to all of the nodes of a given void. At each time step, pressure in full voids was changed based on the flux from its boundary (lumped capacitance), as follows:

$$\Delta P_i = (K_{\mathrm{liq}} \Delta t / V_{\mathrm{void}}) \times \mathrm{sum}(A_j J_j) \tag{S9}$$

where ΔP_i is the change in pressure of the ith void, K_{liq} is the bulk modulus of the liquid, Δt is the time step, V_{void} is the void volume, A_j is the cross-sectional area, J_j is the flux for the jth boundary nodes of the void. At each time step of the calculation, we evaluated $\Sigma(P_i)$ for each void. If $\Sigma(P_i)$ was greater than a random number pulled from a uniform distribution

between 0 and 1, then that void cavitated and starts emptying. During emptying, the pressure at the void-node was held at p_{sat} (representing the small, positive saturation pressure associated with vapor-liquid coexistence in the void), and we calculated the flow leaving the void. Emptying ended when the volume lost equals the total volume of the void. All nodes associated with an empty void varied according to the FD scheme.

B. Choice of simulation parameters

The porosity and permeability of porous silicon used in the code were chosen to match experiments. First, they reproduced the shape of the exclusion zone, from which the value of the poroelastic constant $C \simeq 5 \times 10^{-8}\,\mathrm{m}^2/\mathrm{s}$ was deduced. Then, the porosity $\phi = 0.6$ was adjusted to obtain the right average emptying time. This allowed for the calculation of the value of permeability $\kappa \simeq 1.4 \times 10^{-17}\,\mathrm{m}^2/(\mathrm{Pa.s})$ from the expression $C = \kappa K_{\mathrm{liq}}/\phi$ with $K_{\mathrm{liq}} = 2.2$ GPa.

For simplicity, the voids were considered as cuboids (dimensions $L \times L \times H$) of the same volume as the cylindrical voids of diameter d and depth h fabricated in our samples. We used $L = d$ and set H so that $\pi(d/2)^2 h = L^2 H$.

C. State diagram of drying dynamics obtained from the simulations

The different spatio-temporal drying patterns were explored with our code in the same way as in our experiments presented in the manuscript (Fig. 4).

The transport properties (permeability $\kappa = 1.44 \times 10^{-17}\,\mathrm{m}^2/(\mathrm{Pa.s})$ and porosity $\phi = 0.6$) and cavitation kinetics parameters ($\sigma = 0.0190$, $\Delta\sigma/\sigma = 2.5\%$) were kept constant for all simulations. The parameters that were varied were 1) the geometry of the samples (diameter, depth and spacing of the voids) and 2) the boundary pressure (P_{b}), all of them being set to be the same as in the experiments shown on Fig. 4 in the main text.

As can be seen by comparing Fig. 4 from the main text and Fig. S2, the agreement is excellent between the simulations and our experiments. The shape of the spatio-temporal diagrams (Δr vs. Δt) is well reproduced, showing exclusion zones of similar shapes as the ones obtained experimentally in all quadrants of the phase diagram. The evolution of the front roughness is also well captured. The slight differences that exist between the

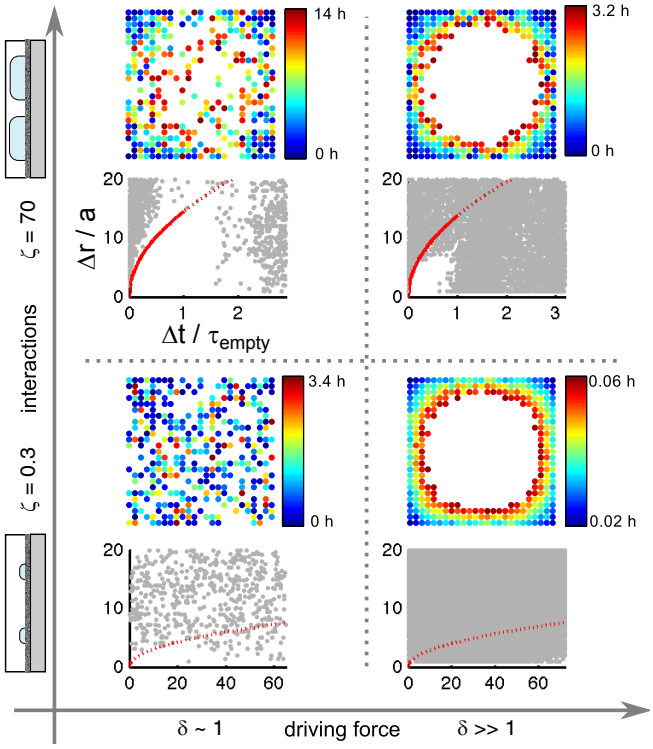

FIG. S2. Reproduction of the experiments of Fig. 4 from the main text using our simulations. See text (section VI C) for details.

experimental and numerical results would possibly be further reduced with a finer tuning of the code parameters, by taking into account some variability from sample to sample. We also note that the shapes of the voids are cylindrical in the experiments and cuboidal in the simulations.

D. Supplemental Movie

We provide a supplemental movie of the simulation from which the snapshots of Fig 3a–d of the main text and the data of the top left panel of Fig. S2 are taken. The movie shows the evolution of the pressure field inside the sample (the colorbar is shown on Fig. 3a) during drying, from an initial pressure of -7 MPa inside the sample and a boundary pressure set to $P_\mathrm{b} = -24$ MPa, corresponding to the pre-equilibration of the sample at 95% relative humidity and a drying at 84% relative humidity, respectively.

Individual frames of the movie were taken at 20 seconds interval of physical time in the

simulation, and the movie is played at 15 fps, entailing an acceleration ratio of 300. Only the first 10 hours (out of 30) are shown here.

---

[1] T. D. Wheeler and A. D. Stroock, Nature **455**, 208 (2008).

[2] J. Chirife and S. L. Resnik, Journal of Food Science **49**, 1486 (1984).

[3] E. P. Barrett, L. G. Joyner, and P. P. Halenda, J. Am. Chem. Soc. **73**, 373 (1951).

[4] A. Rogacs, J. E. Steinbrenner, J. A. Rowlette, J. M. Weisse, X. L. Zheng, and K. E. Goodson, Journal of Colloid and Interface Science **349**, 354 (2010).

[5] F. Caupin and E. Herbert, Comptes Rendus Physique **7**, 1000 (2006).

[6] F. Caupin and A. D. Stroock, "The stability limit and other open questions on water at negative pressure," in *Liquid Polymorphism*, edited by H. E. Stanley (John Wiley & Sons, Inc., 2013) pp. 51–80.

[7] P. G. Debenedetti, *Metastable Liquids: Concepts and Principles*, edited by J. M. Prausnitz and L. Brewer (Princeton University Press, 1996).

[8] K. Davitt, A. Arvengas, and F. Caupin, EPL (Europhysics Letters) **90**, 16002 (2010).

[9] T. D. Wheeler and A. D. Stroock, Langmuir **25**, 7609 (2009).

[10] J. Bear, *Dynamics of Fluids in Porous Media* (Courier Dover Publications, 1988).

[11] M. A. Biot, Journal of Applied Physics **12**, 155 (1941).